Programmable Shape Change in Semicrystalline Liquid Crystal Elastomers

Mahjabeen Javed[1], Tyler Corazao[2], Mohand O. Saed[3], Cedric P. Ambulo[4], Yuzhan Li[5], Michael R. Kessler[6], and Taylor H. Ware[1,2]*

[1] *Department of Biomedical Engineering, Texas A&M University, College Station, Texas 77843, USA*

[2] *Department of Materials Science and Engineering, Texas A&M University, College Station, Texas 77843, USA*

[3] *University of Cambridge, Cambridge, CB2 1TN, UK*

[4] *Air Force Research Laboratory, Dayton, Ohio, 45433, USA*

[5] *University of Science and Technology Beijing, Beijing, 100083, China*

[6] *North Dakota State University, Fargo, ND, 58108, USA*

Keywords: Liquid crystal elastomers, actuator, stimuli-responsive, polymers, crystallization.

ABSTRACT

Liquid crystal elastomers (LCEs) are stimuli-responsive materials capable of reversible and programmable shape change in response to an environmental stimulus. Despite the highly responsive nature of these materials, the modest elastic modulus and blocking stress exhibited by these actuating materials can be limiting in some engineering applications. Here, we engineer a semicrystalline LCE, where the incorporation of semicrystallinity in a lightly-crosslinked liquid crystalline network yields tough and highly responsive materials. Directed self-assembly can be employed to program director profiles through the thickness of the semicrystalline LCE. In short, we use the alignment of a liquid crystal monomer phase to pattern the anisotropy of a semicrystalline polymer network. Both the semicrystalline-liquid crystalline and liquid crystalline-isotropic phase transition temperatures provide controllable shape transformations. A planarly aligned sample's normalized dimension parallel to the nematic director decreases from 1 at room temperature to 0.42 at 250 °C. The introduction of the semicrystalline nature also enhances the mechanical properties exhibited by the semicrystalline LCE. Semicrystalline LCEs have a storage modulus of 390 MPa at room temperature, and monodomain samples are capable of generating contractile stress of 2.7 MPa on heating from 25 °C to 50 °C, far below the nematic to isotropic transition temperature. The robust mechanical properties of this material combined with the high actuation strain can be leveraged for applications such as soft robotics and actuators capable of doing significant work.

1. INTRODUCTION

Soft, stimuli-responsive polymers have demonstrated great utility as building blocks for dexterous soft robots, actuators, artificial muscles, and dynamic medical devices due to their active and

adaptive nature. These functional materials undergo controlled shape change induced by an array of external triggers such as heat[1,2], light[3,4], solvents[5], and magnetic field[6], translating external energy into mechanical work. Materials like dielectric elastomers[7], hydrogels[8], shape-memory materials[9,10], and liquid crystal elastomers (LCEs)[11,12] have been reported to exhibit programmable macroscopic deformation.

Shape change in responsive materials can be classified as reversible or irreversible. Semicrystalline polymers capable of reversible shape change have been realized, where the responsive mechanism results from crystallization-induced expansion and melting-induced shrinkage, under constant external stress.[10,13,14] The presence of an external load in such cases is imperative as it directs the growth of the crystallites along the uniaxial stretching direction. Semicrystalline actuators have also been developed that can harness reversible actuation in the absence of a persistent external bias or stress. Behl et al. developed polymer networks with two crystallizable switching domains capable of fully reversible macroscopic shape-change in the absence of a bias stress.[15] Another approach to designing stress-free semicrystalline actuators is by designing a bilayer composite consisting of a pre-stretched shape memory polymer film embedded in an unelongated elastomer resulting in built-in stress in the system.[16] The mechanically active nature of these materials makes them of interest for soft robotics and actuators. However, these materials require external manipulation to shape the polymer, referred to as the programming step. This step limits the type of shape change that can be achieved by these materials.

LCEs are another class of soft, functional materials capable of reversible shape morphing in response to an environmental stimulus. These lightly crosslinked polymers couple the orientational order of liquid crystals with the entropic elasticity of elastomers. Shape change is a

result of a change in the order parameter. This type of shape change can be programmed into the polymer network by controlling the molecular orientation within the network prior to crosslinking. Stimuli like heat[17], light[18,19] and solvent[5,20] induce an order-to-disorder transition resulting in the LCE contracting along the nematic director and expanding perpendicular to it.[21] LCEs with programmed molecular orientation were first reported by Finkelmann et al. where the director was aligned by mechanically straining and crosslinking the elastomer.[22] Several approaches have emerged to orient the mesogenic monomers prior to crosslinking, such as field-assisted alignment[23,24] and extrusion-based 3D printing[25,26]. Directed self-assembly of a "command surface" can also be used to spatially pattern molecular order in the LCE. By controlling and locking in a variation of well-defined director profiles within the LCE, complex shape transformation of a monolithic material can be achieved.[24,27]

Due to the low crosslink density and glass transition temperature of LCEs, mechanical properties such as toughness, force output, and strength are compromised, limiting these responsive materials in their engineering applications.[28,29] To achieve higher-performance engineering LCEs, there is a need to improve mechanical properties without compromising the strain associated with the order-disorder transition. Several strategies have been explored to improve the functional properties of LCEs. One approach to increase force output is to simply increase the thickness of the films being prepared, but for many applications such thick actuators may not be appropriate. Furthermore, the surface anchoring strength of the command surface used to program LCEs by directed self-assembly is only effective for films below ~100 μm thick.[30] Crosslink density can also be increased to increase the elastic modulus of the material, but this approach greatly compromises the magnitude of the stimulus response the system can exhibit.[31] Interpenetrating liquid crystalline polymer networks have been developed that significantly

enhance the mechanical properties of the LCE.[32–36] Taking advantage of this approach, Yang et al. reported on interpenetrating polymer networks to achieve blocking stress of 2.53 MPa and work capacity of 1267.7 kJ/m^3.[32] Inducing semicrystallinity in LCEs is another approach to enhance stiffness and achieve tough, higher-performance LCEs.[12,37–39] Kim et al. reported on a crystallizable thiol–acrylate LCE material with blocking stress and actuation work capacity of 1.3 MPa and 730.5 kJ/m^3.[37] Despite the many efforts in developing and processing tough, higher-performance LCEs for use as soft actuators, the complexity of shape change in the above systems is limited. The only way to orient the mesogenic moieties in these systems is through uniaxial stretching, hindering the ability to pattern complex, spatially varied director profiles in the LCE.

Here, we demonstrate highly responsive, shape-programmable semicrystalline LCEs based on thiol-ene photopolymerization, where both liquid crystalline and crystalline phases contribute to shape-change. Directed self-assembly can be used to spatially pattern the nematic director of the LCE precursors. On cooling these oriented LCEs, crystallization occurs resulting in semicrystalline LCEs. By controlling and locking in well-defined director profiles within the LCE, complex shape transformation of a semicrystalline LCE can be achieved. The synergistic combination of semicrystallinity and liquid crystallinity in a monolithic element not only retains the highly responsive nature of LCEs but also increases the force output and toughness of these shape changing materials.

2. MATERIALS AND METHODS

2.1. Materials

The liquid crystal monomers 1,4-phenylene bis(4-(hex-5-enyloxy)benzoate) (Monomer 1) and 2-methyl-1,4-phenylene bis(4-(hex-5-enyloxy)benzoate) (Monomer 2) were purchased from

SYNTHON Chemicals GmbH & Co. KG. Thiol crosslinker pentaerythritol tetrakis(3-mercaptopropionate) (PETMP), chain extenders 2,2′-(ethylenedioxy) diethanethiol (EDDT) and 1,9-Nonanedithiol (NDT), and photoinitiator Irgacure 1-369 were purchased from Sigma-Aldrich. Brilliant yellow dye was purchased from Sigma-Aldrich. Chloroform, dimethylformamide, acetone, and isopropanol were obtained from Fisher-Scientific.

2.2. Synthesis and Preparation

LCE samples were synthesized by thiol-ene click reaction. For preparing semicrystalline LCEs, a mixture of monomer 1, crosslinker, and chain extender with 1.5 wt% of the photoinitiator (Figure 1A) was heated and vortexed for homogenous mixing. The monomer mixture was then filled into a mold constructed out of two glass slides through capillary action at 115 °C, at which the mixture is in its nematic state. For making aligned non-crystalline LCE films, a mixture of monomer 2, crosslinker, and chain extender was filled into the mold in its nematic state at 65 ˚C. The mold was irradiated with a 365 nm UV light (Lumen Dynamics, OmniCure LX400+) with an intensity of 8 mW/cm^2 for 150 seconds on each side to initiate photopolymerization. Intensity was measured using ABM-USA, Inc. Intensity Meter. LCE samples were post-cured at 120 ˚C overnight to complete the reaction. To synthesize LCEs with varying degrees of crystallinity, the LC monomer 1 was partially or fully replaced with the bulkier methylated monomer 2, and LCE films were synthesized in a similar manner. In all films, the molar ratio of thiol functional groups to alkene functional groups was 1:1.

2.3. Photoalignment

To induce molecular alignment in the LCE, glass molds were constructed using glass slides coated with a photo-responsive dye. Glass slides (75 mm × 51 mm × 1.2 mm, Electron Microscopy

Sciences) were sequentially rinsed with acetone, isopropanol, and deionized water, and treated with oxygen plasma for 1 minute. A photo-alignable solution was prepared by mixing 1 wt% of brilliant yellow in dimethylformamide, filtered through a 0.2 μm pore size filter, and spin-coated on the cleaned glass slides at 750 rpm (1500 rpm/s) for 10 s and 1500 rpm (1500 rpm/s) for 30 s. Coated slides were baked at 90 ˚C for 30 minutes and then selectively patterned by exposure to linearly polarized light through a modified projector, at an intensity of 10 mW/cm^2 (Vivitek D912HD) for 2 minutes. A glass mold was assembled using the patterned glass slides, with a 50 μm spacer in between the two slides.

2.4. Thermal Characterization

Differential scanning calorimetry (DSC) was performed using a TA Instruments Q-20. Samples of approximately 5 mg were loaded into standard aluminum DSC pans and heated from room temperature to 170 °C, cooled to -15 °C, and then heated to 170 °C at fixed rates of ±10 °C/min, except for Figure S5 where the temperature ramp rates are varied from ±2 °C/min to ±20 °C/min. The first cooling and second heating scans are shown (Figure 2A,C, Figure S1C, S2B, S4B,C, S5, S6 Supporting Information). Thermal analysis for each composition was repeated 3 times (n = 3).

2.5. Mechanical characterization

Mechanical analysis of the materials was carried out by a dynamic mechanical analyzer (DMA) (TA Instruments, RSA-G2). For quasi-static tensile testing, planarly aligned LCEs were prepared. Rectangular strips of dimensions approximately 20 mm x 3 mm x 0.05 mm were loaded and stretched at a constant linear rate of 0.1 mm/s. To measure blocking stress, a constant strain of 0.01% strain was used while the temperature was ramped from 25 °C to 200 °C with a 3.0 °C/min ramp rate. Past this temperature majority of the samples broke during the test. For cyclic blocking

stress measurements, the temperature was ramped from 25 °C to 50 °C and back to 25 °C four times at a rate of 1.0 °C/min after an initial heat-cool cycle. For cyclic actuation strain measurements, 0 N force was maintained to an LCE sample while the temperature was ramped from 25 to 50 °C with a 1.0 °C/min, for four heat-cool cycles. Before the test, samples were heated up to 100 °C and allowed to cool down without confinement. For dynamic mechanical analysis, polydomain test specimens were prepared of dimensions approximately 20 mm x 3 mm x 1 mm and tested in tensile mode at 0.2% strain at 1 Hz and heated from -30 to 180 °C at a rate of 3.0 °C min^{-1}. All tests were repeated three times for each composition (n = 3).

2.6. Gel Fraction

LCE films of varying crosslinker content were weighed to obtain an initial mass ($M_{initial}$). Samples were immersed in 20 ml chloroform for 48 hours at room temperature. The solvent was extracted by first air drying the samples for 24 hours and then vacuum drying at 60 °C for 48 hours until a final mass (M_{final}) is achieved. Gel fraction was obtained using the final equation:

$$Gel\ Fraction\ (\%) = \frac{M_{final}}{M_{initial}} \times 100\%$$

All gel fraction tests were repeated three times (n = 3) for each composition.

2.7. Optical Properties and Actuation Performance

Optical properties of the samples were analyzed under a polarized optical microscope (Nikon ECLIPSE LV100N POL). To analyze the actuation behavior of monodomain samples, a thermal stage (Linkam) was used to control the temperature. Planarly aligned LCE samples were cut and placed on a glass slide with silicone oil to prevent adhesion. The sample was placed in the sample

holder on the thermal stage, and shape change was observed from 23 °C to 250 °C. Shape change along the nematic director (contraction) was measured using the following equation:

$$Contraction = \frac{L}{L_0}$$

where L_0 is the initial length and L is the final length.

Shape change perpendicular to the nematic director (expansion) was measured using the following equation:

$$Expansion = \frac{L}{L_0}$$

where L_0 is the initial width and L is the final width.

To achieve out-of-plane shape change at room temperature, aligned samples, released from the glass mold, were first heated up to 100 °C past their crystalline melt and then allowed to cool back down to room temperature. This ensures any built-in stress in the polymers from being confined between two glass slides is released and the samples are free to adopt their programmed 3D shape on cooling. Thermal stimulus-response of twisted helical structures was imaged and quantified. Helical samples of dimensions 15 mm x 1 mm x 0.05 mm are heated from 23 °C to 250 °C in a silicon bath and imaged for actuation analysis. Actuation tests were repeated 3 times (n = 3). Macroscopic shape changes in cones and anti-cones in response to heat were also imaged. Azimuthally and radially aligned samples are heated from 23 °C to 180 °C and imaged. Each 3D structure was immersed in a silicon oil bath that was heated using a hotplate. Temperature within the oil bath was measured using a thermocouple (Traceable Total-Range thermocouple). The 2x3

array of radial defects was imaged at room temperature without a silicon bath. Images of the actuation behavior were taken using a digital single-lens reflex (DSLR) camera (Nikon).

2.8. X-ray Diffraction

For small-angle X-ray experiments, Rigaku S-MAX 3000 (Soft Matter Facility, College Station, Texas) was used. Cu Kα X-rays (wavelength 1.54 Å) were generated from a RA-Micro7 HFM rotating anode operating at 40 kV and 30 mA. Diffraction patterns were obtained over a 2θ range of 0.6° to 3.5°. Each sample was measured for 3 hours. 2D spectra were converted to a 1D plot using SAXSGUI software. For wide-angle X-ray experiments, Bruker-axs D8 Advanced Bragg-Brentano X-ray Powder Diffractometer (X-ray Diffraction Laboratory, College Station, Texas) was used. Cu Kα X-rays (wavelength 1.54 Å) were generated from a Cu anode at 40 kV and 25 mA. Diffraction patterns were obtained over a 2θ range of 3° to 70°. Each sample was measured for 60 minutes. Diffraction patterns were collected twice for each sample type. The areas of multiple crystalline peaks as well as the amorphous halo were calculated in Origin Pro, and percent crystallinity was calculated using the following equation:

$$Crystallinity\ (\%) = \frac{Area\ under\ crystalline\ peaks}{Area\ under\ crystalline\ peaks + Area\ under\ amorphous\ halo} \times 100$$

3. RESULTS AND DISCUSSION

Semicrystalline LCEs were synthesized by employing thiol-ene click chemistry-based photopolymerization. Figure 1A depicts the molecular structures of the monomers being employed. Inspiration for this synthetic strategy comes from several previous reports that explored thiol-ene reactions to synthesize LCEs.[40–43] Prior synthetic strategies have been shown to yield

LCEs that later undergo crystallization. However, those approaches are not suitable for surface alignment. For example, if the reaction proceeds too quickly as is the case for some thiol-acrylate Michael addition reactions, the precursors are unable to surface align in the nematic phase prior to gelation.[12,37,39] However, this synthetic route is novel in that it yields semicrystalline LCEs and is also sensitive to surface alignment strategies, allowing for complex shape change to be programmed into the LCE.

A divinyl nematic monomer (monomer 1) is mixed with an isotropic dithiol chain extender and a tetrathiol crosslinker. The symmetry of this linear divinyl mesogenic monomer encourages homogenous chain packing, resulting in crystallization. This monomer is different than some commonly reported diacrylate-functionalized reactive mesogens to synthesize LCEs in that diacrylate monomers homopolymerize, introducing a higher degree of crosslinking and heterogeneity in the polymer network.[41,44] A different dithiol spacer, NDT, can also be utilized to achieve semicrystalline networks with similar properties (Figure S1, Supporting Information). Table S1 details the chemical formulations of all LCEs reported (Supporting Information).

The mesomorphic behavior of the LC mixture prepared with 40 mol% thiol crosslinker is shown in Figure S2A, Supporting Information. Near 120 °C, a nematic phase is observed after melting of crystallized monomer mixture as denoted by the typical Schlieren texture.[41] Above 170 °C, nematic to isotropic transition (T_{ni}) was observed as noted by the absence of birefringence and by a small endothermic peak in the DSC thermogram of the monomer mixture (Figure S2B, Supporting Information). The LC monomer mixture can be readily filled in a surface-aligned glass mold in the nematic phase and adopts the alignment as dictated by the command surface (Figure 1B). After radical polymerization by UV exposure, crosslinked films are obtained. On cooling, these nematic elastomers crystallize, yielding stiff semicrystalline LCEs.

The crystallinity of the system can be modulated by reducing the symmetry of the monomers with the introduction of a methyl group to the mesogenic core, as seen by monomer 2 in Figure 1A.[45,46] Crystallization is known to impart mechanical strength and toughness to the polymer network.[37,39,47,48] By tuning chain packing and concurrently crystallinity, the widely different mechanical properties of the resultant films could be observed.[39] Semicrystalline LCEs synthesized from the symmetric divinyl monomer (monomer 1) result in a rigid polymer network while analogous LCEs made from the methylated counterpart (monomer 2) lack crystallinity, leading to low-modulus elastomers (Figure S3, Supporting Information).

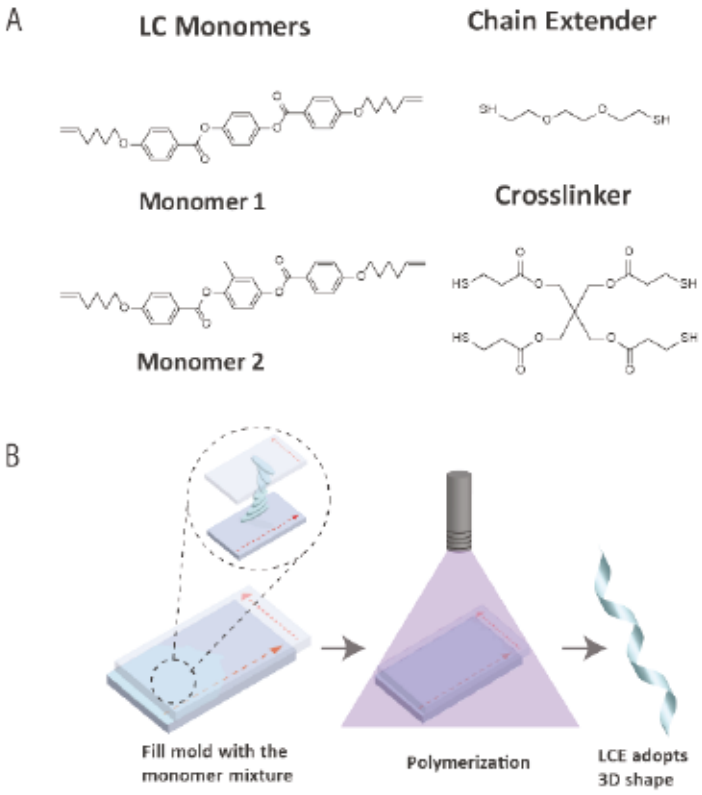

Figure 1. (A) Chemical structures of the LC monomers, chain extender, and crosslinker. (B) Schematic of the process used to synthesize aligned and crosslinked LCEs.

LCEs of varying crosslinking density were synthesized by altering the ratio between the thiol crosslinker and the thiol chain extender while still maintaining the equimolar ratio between

vinyl groups to thiols. After radical polymerization, the LCE has a gel fraction of 97 ± 0.8% for 40 mol% crosslinker content and 87 ± 1.1% for 20 mol% crosslinker content. Non-crystalline LCEs synthesized with monomer 2 have a gel fraction of 93 ± 1.7% for 40 mol% crosslinker content and 93.7 ± 3.2% for 20 mol% crosslinker content (Figure S4A, Supporting Information).

Networks synthesized with monomer 1 are semicrystalline in nature at room temperature. The thermal properties of these semicrystalline LCEs were explored using differential scanning calorimetry. Figure 2A shows the DSC thermogram of the first cooling cycle of semicrystalline LCEs with varying crosslinker content. All semicrystalline LCEs exhibit an exothermic crystallization peak upon cooling, which becomes more pronounced with a decrease in crosslink density. The enthalpy of crystallization increases from 13.3 ± 1.3 J/g for 40 mol% crosslinker content to 19.9 ± 0.2 J/g for 0 mol% crosslinker content (Figure 2B). This indicates a progressive reduction in the degree of crystallinity with increasing crosslink density. For 20 and 0 mol% crosslinker content, a second exothermic peak on cooling can be seen, attributed to a first-order isotropic to nematic transition. At higher crosslink density, the transition from nematic to paranematic becomes second order in nature, as has been previously described.[49–51] Endothermic melting peaks are also observed during the second heating cycle (Figure S4B, Supporting Information). Interestingly, the more highly crosslinked LCEs exhibit fast kinetics of crystallization with the hysteresis between the crystalline and melting phase change ranging from 5.6 ± 1.9 °C for 40 mol% crosslink density to 38.1 ± 0.8 °C for 0 mol% crosslink density. This phase transition hysteresis for semicrystalline LCEs with 40 mol% crosslink density remains unchanged for different temperature ramp rates, further supporting the fast crystallization kinetics (Figure S5, Supporting Information). After cooling to room temperature, the semicrystalline

LCEs do not exhibit a time-dependent crystallization behavior, and samples synthesized with 40 mol% PETMP remained unchanged after 5 days of storage (Figure S6, Supporting Information).

Analogous LCEs that do not crystallize were also synthesized to examine the properties imparted upon the polymer network due to the inclusion of crystallinity. Here, the rigid core of the previously used monomer is modified by adding a methyl group. This methyl group disrupts the regularity and symmetry of the polymer chain packing, thereby reducing the tendency for crystallinity. LCEs were synthesized by varying the ratios between the methylated and unmethylated LC monomer, which affords further control over crystallinity. Figure 2C shows DSC thermograms of LCEs with increasing concentration of the methylated monomer and the associated changes in enthalpy. As the concentration of the methylated monomer is systematically increased from 0 mol% to 100 mol%, enthalpy decreases from 13.4 ± 1.1 J/g to 0 J/g (Figure 2D). As the degree of crystallinity decreases, so does the temperature at which the crystallization and melting peaks occur, until 30 mol% at which point no crystallization is observed (Figure 2C, S4C, Supporting Information). It is worth noting that even though the crystallinity in the system is quenched, the system is not entirely amorphous and still contains liquid crystalline order.

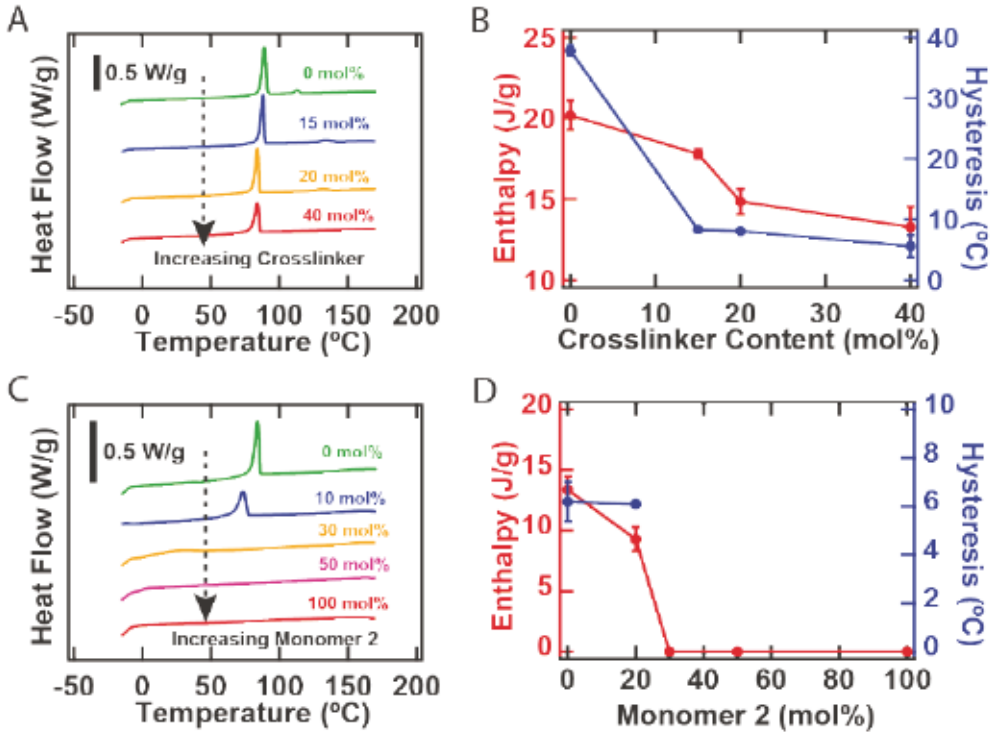

Figure 2. (A) DSC thermograms of the first cooling cycle of semicrystalline LCE samples while varying the crosslinker content. (B) Enthalpy and hysteresis as a function of crosslinker content for semicrystalline LCE. (C) DSC thermograms of LCE samples with varying concentrations of monomer 2. (D) Effect of monomer 2 on the enthalpy and hysteresis of the polymer network. N = 3 for all tests.

Wide-angle X-ray scattering (WAXS) and small-angle X-ray scattering (SAXS) further confirm the presence of an ordered crystalline network in the semicrystalline LCE (Figure 3A,B). 1D WAXS diffraction plot of semicrystalline LCEs exhibit two narrow peaks at 19.9° and 21.1° and two smaller peaks at 27.5° and 36.9°. These results roughly correspond with peaks of previously reported crystallizable LCEs.[12,37] Semicrystalline LCEs exhibit around 50% crystallinity (n=2), as determined by WAXS. A peak at 2.7° is also seen for semicrystalline LCEs in the 1D SAXS profile, while no peak is evident for the non-crystalline LCE. 2D SAXS pattern shows a four-spot pattern for the semicrystalline LCE, each spot separated by 90°, that may be

associated with short-range smectic-C type fluctuations, while this pattern is not visible for the non-crystalline LCE.[52–54] We note that the higher-order present is not simply associated with the smectic mesophase in the LCE system because of the high rigidity exhibited by the semicrystalline LCE and the high enthalpy associated with melting from the semicrystalline to liquid crystalline phase.

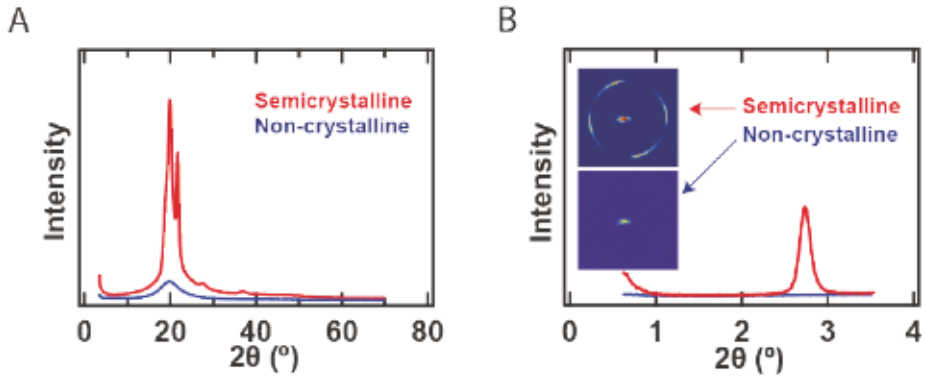

Figure 3. (A) Wide-angle X-ray Scattering (WAXS) for semicrystalline and non-crystalline LCEs. **(B)** 2D and 1D small-angle X-ray Scattering for semicrystalline and non-crystalline LCEs. Each test was repeated 2 times.

The chemistry being adopted to synthesize semicrystalline LCEs is amenable to surface alignment strategies, where directed self-assembly of a command surface can be used to orient the nematic phase of the monomer solution. The ability to orient these materials using directed self-assembly is distinct from previously described approaches that generate LCEs capable of crystallization, where alignment was achieved via mechanical stretching. Importantly, it is difficult to orient any class of semicrystalline polymers without using mechanical load or flow.[14,47,55] For example, Vectra, a high-performance crystallizable liquid crystal polymer, is oriented during injection molding or extrusion techniques, where the mesogens orient themselves in the direction of flow.[47,56,57] In this study, directed self-assembly allows for precise spatial and

hierarchical control of both the molecular orientation and the programmed mechanical response in semicrystalline polymers.

Compositions with 40 mol% crosslinker content were utilized to synthesize monodomain semicrystalline and non-crystalline LCE films. A dichroic azobenzene-based dye was coated onto glass slides and subsequently patterned by selective exposure to linearly polarized light. The photoinduced orientation of this dye ultimately dictates the director profile within the LCE as well as the mechanical response (Figure 4A). Polarized optical microscopy was used to confirm the homogenous molecular alignment of the samples (Figure 4B). The programmed mechanical anisotropy within the material results in dramatic shape change, where heating the aligned samples leads to contraction along the nematic director and expansion orthogonal to it. Semicrystalline LCE shows maximum actuation behavior past the nematic-to-isotropic phase transition where the normalized dimension parallel to the nematic director decreases from 1 at room temperature to 0.42 ± 0.02 at 250 °C and normalized dimensions perpendicular to the nematic director increase from 1 at room temperature to 1.53 ± 0.11 at 250 °C (Figure 4C). Non-crystalline LCE samples also exhibit heat-induced actuation behavior (Figure 4D). Parallel to the nematic director, the normalized dimension decreases from 1 at room temperature to 0.59 ± 0.03 at 250 °C, and normalized dimensions perpendicular to the nematic director increase from 1 at room temperature to 1.44 ± 0.06 at 250 °C. Here, shape change is quantified by the contracted length or elongated width normalized to the length or the width of the LCE at room temperature (L/L_0).

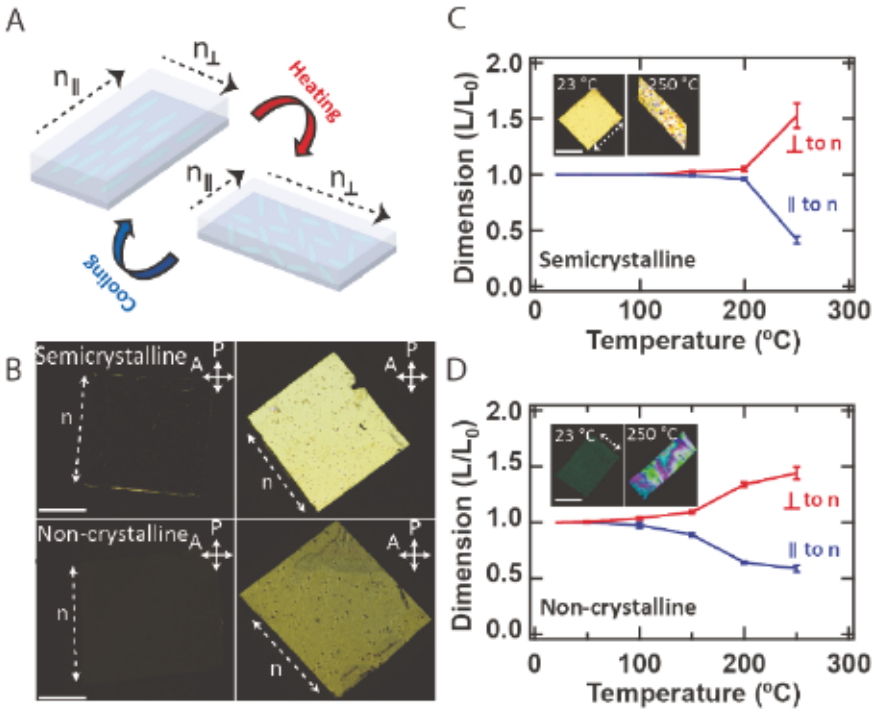

Figure 4. (A) Schematic of a planarly aligned monodomain LCE samples anisotropically actuating in response to temperature. LCE contracts along the nematic director and expands perpendicular to it. **(B)** Polarized optical micrograph images of planarly aligned semicrystalline and non-crystalline LCEs. **(C, D)** Dimensional changes of aligned semicrystalline and non-crystalline LCEs along and perpendicular to the nematic director as a function of temperature. Arrows indicate the nematic director orientation. For plots C, and D each data point represents the mean (n = 3), and the error bars represent the standard deviation. Scale bar = 500 μm.

Repeated thermal cycling of both semicrystalline and non-crystalline LCE demonstrates reversibility of the actuation behavior (Figure 5). LCEs were cycled 9 times between 23 °C to 250 °C. After the first heating cycle, semicrystalline LCE samples show an approximately 20% loss in sample length, but shape change after this first heating cycle is reversible (Figure 5A). This irreversible shape change may be attributed to a recovery of stresses trapped by crystallization.

Non-crystalline LCE samples do not exhibit this same loss in sample length, and shape change here is fully reversible over the repeated thermal cycles (Figure 5B). The normalized volume of the semicrystalline LCE increases on melting the crystalline domains and exhibits an irreversible change in volume on the first thermal cycle. The volume of the non-crystalline LCE remains nearly the same during heating and cooling, as is expected for LCEs.[21] The normalized volume, as compared to the initial volume of each sample after crosslinking, for semicrystalline LCE at room temperature decreases from 1 to 0.87 ± 0.03 after the first heating and cooling cycle. The origin of this irreversible volume change is unclear, but it may be due to rearrangement of the crystalline fraction of the network.[58,59] In subsequent cycles, the normalized volume increases on heating from 0.87 ± 0.03 to 0.96 ± 0.06 at 250 °C. On cooling, the normalized volume returns to the value observed after the first heating and cooling cycle. The reversible increase in volume after the first cycle during heating is expected for semicrystalline networks on heating.

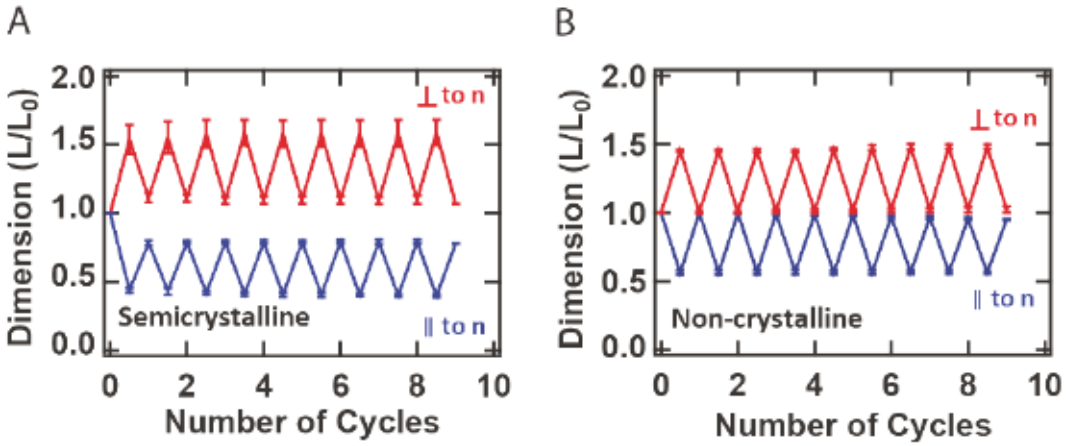

Figure 5. (A, B) Dimensional changes of aligned semicrystalline and non-crystalline LCEs when cycled 9 times between 23 °C to 250 °C. Each data point represents the mean (n = 3), and the error bars represent the standard deviation.

Storage modulus and dissipation factor were measured as a function of temperature for different crosslinker contents (Figure 6A,B). Several thermomechanical transitions can be

observed. The semicrystalline LCEs each show a drop in storage modulus heating through T_g and T_m. Samples synthesized with 40 mol% crosslinker have a T_g of -4 ± 1.6 °C. After being heated through T_g and T_m, the network containing 40 mol% crosslinker reached a stable rubbery plateau at around 11 ± 2 MPa, denoting a well crosslinked polymer network. Semicrystalline LCEs with 20 mol% and 15 mol% crosslinker content exhibit a further drop in modulus on heating through the T_{ni}. This drop in the modulus above T_{ni} is typically associated with LCEs crosslinked in the isotropic state.[12,60,61] Although no flow in materials is seen, above T_{ni} the samples become too compliant to measure modulus reliably. It is likely that in these networks, 20 mol% and 15 mol% crosslinker contents are insufficient to fully form a polymer network, in agreement with the relatively lower gel fraction of these materials. For an isotropic rubber, it is expected to see the rubbery modulus increase with temperature, however, it is likely that there is an ongoing reduction in order in the LCEs over the entire temperature range shown which precludes the modulus from increasing. The presence of this remnant order can be more clearly seen from the actuation behavior shown in Figure 4C and Figure 5A where the semicrystalline LCE sample shows actuation up to 250 °C. Above 200 °C, samples with 40 mol% PETMP that were loaded in the DMA fractured, which prevents the full range of viscoelastic behavior from being captured. This is not due to flow of the polymer as no flow was observed in the POM. We also note that the network with 40 mol% PETMP has a gel fraction of 97 ± 0.8% (Figure S4A).

The inclusion of the methylated monomer into the polymer network affords control over the crystallinity of the system and concurrently its mechanical properties. Figure 6C,D show the storage modulus and tan delta as a function of temperature for LCEs with varying amounts of the methylated monomer while keeping the crosslinker content constant at 40 mol%. Gradual reduction of storage modulus at room temperature can be seen with an increase in the concentration

of the unmethylated monomer. The differences in the rubbery moduli of these films despite the similar crosslinker content may be due to the differences in the reactivity of the two monomers as well as the differences in the order parameter. For semicrystalline LCEs synthesized entirely with monomer 1, shape change is still seen at up to 250 °C, signifying retention of the LC order in these films even at those high temperatures (Figure 4C). All films tested, exhibit a pronounced drop in storage modulus with increasing temperature, but the temperature onset at which this drop occurs depends strongly on if the network is semicrystalline or not. In compositions without crystallinity, there is a sharp drop in modulus as the temperature approaches T_g. For semicrystalline formulations, this drop is exhibited only after the material is heated through both T_g and T_m. Aligned semicrystalline LCEs also exhibit mechanical anisotropy (Figure S7). While semicrystalline materials are known to be anisotropic after drawing, we note that the anisotropy in these materials was dictated by directed self-assembly. Young's modulus may be slightly higher when the director profile is along the loading axis (90°) than when its perpendicular to it (0°) (Table S2, Supporting Information). Failure strain is highest for samples when the nematic director is at 0°. Likely this increased failure strain can be attributed to the reorientation of the nematic director and/or crystallites in the strain direction, allowing the sample to elongate considerably before fracture.[31,62]

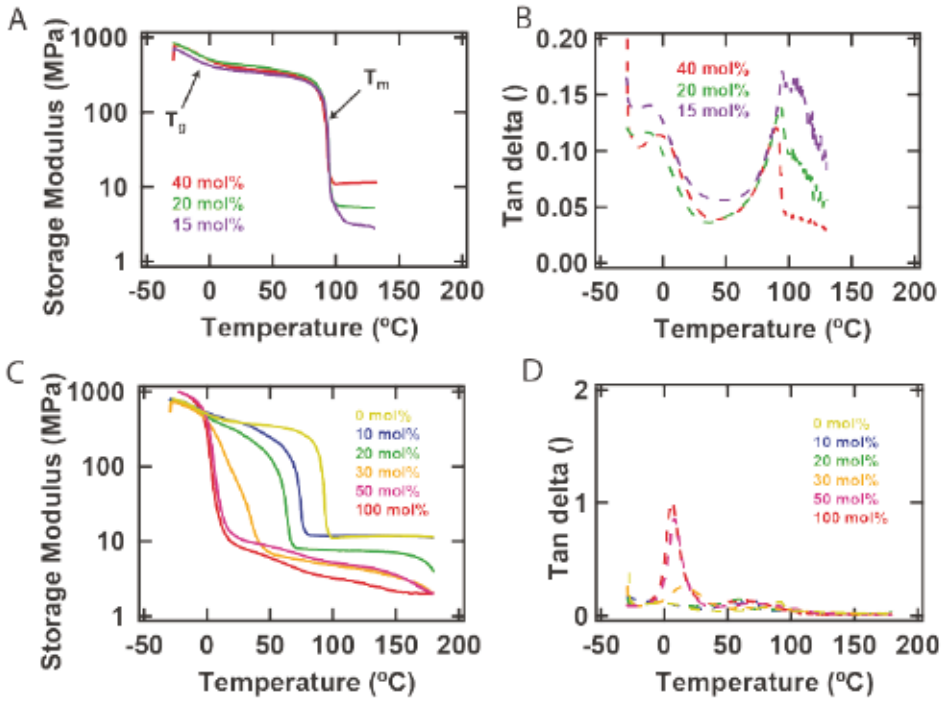

Figure 6. (A) Storage Modulus as a function of temperature for semicrystalline LCEs with varying degrees of crosslinker content. **(B)** Tan delta as a function of temperature for semicrystalline LCEs with varying degrees of crosslinker content. **(C)** Storage Modulus as a function of temperature for LCEs synthesized with varying amounts of monomer 2. **(D)** Tan delta as a function of temperature for LCEs with varying amounts of monomer 2. N = 3 for all tests.

The inclusion of crystallinity enhances the mechanical properties of the material and the material's ability to generate stress. Weights were hung on polydomain 50 μm thick semicrystalline and non-crystalline LCE samples (Figure 7). Semicrystalline LCE can support 0.5 MPa without dramatically changing its initial shape while the compliant, non-crystalline LCE stretches considerably. Blocking force was measured using iso-strain measurement (Figure 8A). Here a monodomain LCE was clamped in tension, while the temperature is increased. As the sample undergoes phase transition, it generates contractile stress. The semicrystalline LCE exhibits unique behavior where it generates strong contractile stress at temperatures far below the

nematic-to-isotropic transition. This may be due to the contraction of tie molecules[63], the partial melting of the crystallites, or other order to disorder phase change such as a small reduction of order of the nematic phase. Contractile stress of 2.7 ± 0.03 MPa is generated over a temperature window of 25 °C to 50 °C (Figure 8A,B) demonstrating the potential of the material to be used for small strain, higher stress, low hysteresis actuators. LCE materials generating higher blocking stress have been reported. To our knowledge, there are no reported LCEs capable of generating this high blocking stress at such low temperature values and over such a narrow temperature range.[32,35,37,64] Actuation strain of an unconstrained semicrystalline LCE sample was also measured using an iso-force test (Figure 8C). On heating up to 50 °C, LCE films exhibit an actuation strain (contraction) of 0.56 ± 0.07 % along the nematic director. The average coefficient of thermal expansion (CTE) generated by the oriented semicrystalline LCEs is -224 ppm/°C. This value is substantially larger in magnitude than the CTE observed in oriented semicrystalline polymers like high density polyethylene and nylon that have been previously reported for high-stress artificial muscle applications.[65–68] Such polymers exhibit high blocking stress at high temperatures but show very minimal blocking force and actuation strain in the small temperature window between room temperature and 50 °C. Low density polyethylene may have similar negative CTE to the semicrystalline LCEs in this temperature range.[63] Semicrystalline LCEs not only demonstrate high blocking stress and a negative thermal expansion over a temperature window of 25 °C to 50 °C, but they are also capable of programmable shape deformation, making them ideal for higher stress actuators operating at low-temperature windows. Upon further heating, the expansion in the material results in a decrease in this blocking stress until the crystalline melt transition is completed. As the material approaches the nematic-to-isotropic transition, blocking stress of 0.8 ± 0.02 MPa is generated past the nematic to isotropic transition. In contrast, the non-

crystalline LCE does not exhibit these multiple transitions and is only able to generate a single blocking stress peak of 0.4 ± 0.1 MPa at 200 °C, due to melting of the nematic phase (Figure 8A).

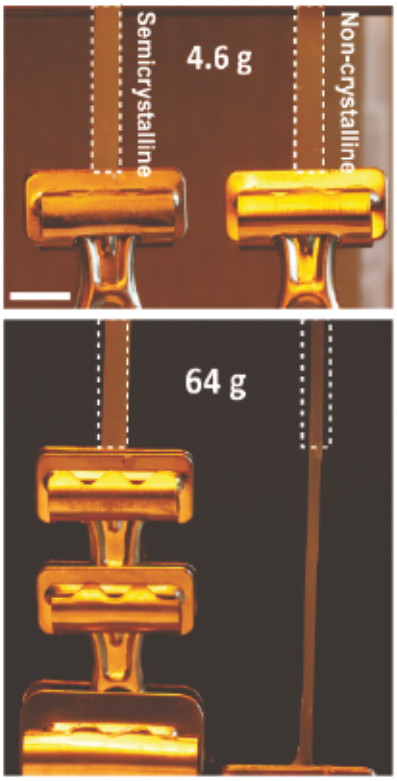

Figure 7. Polydomain semicrystalline and non-crystalline LCEs with load. Semicrystalline rigid LCE shows no deformation while the compliant non-crystalline LCE stretches significantly in response to the increasing load (Scale bar = 10 mm).

By patterning director profiles within the semicrystalline LCE, out-of-plane deformation of the rigid, aligned samples can be realized. Programming a 90° twist in the director profile through the thickness of the LCE results in twisted helical structures (Figure 9A,B). The semicrystalline LCEs are crosslinked at an elevated temperature, that is above the T_m but below the T_{ni}. This programs them to be flat at the crosslinking temperature and adopt their predetermined 3D shape as a result of cooling from that crosslinking temperature (Figure 9C). The number of

twists is dependent on the aspect ratio, with strips of smaller widths showing a higher number of twists, as observed in related materials.[69]

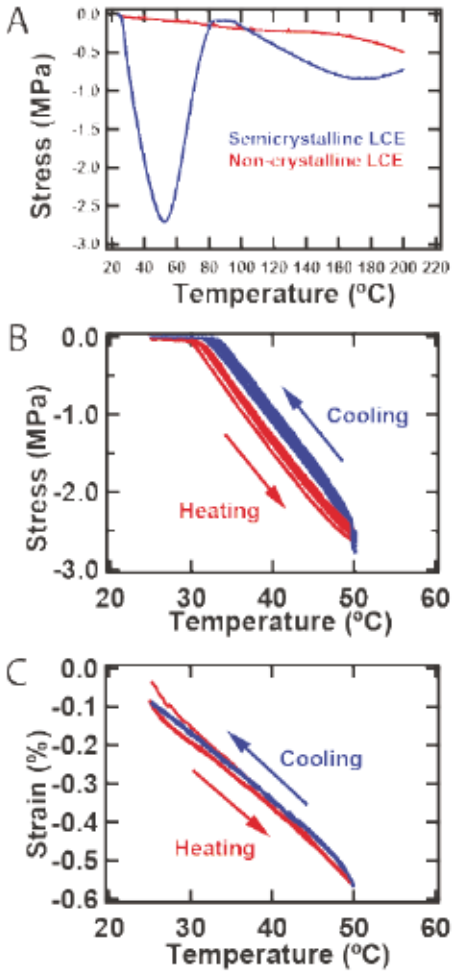

Figure 8. (A) Iso-strain (0.01%) measurements of aligned semicrystalline LCE and aligned non-crystalline LCE. **(B)** Iso-strain tests for semicrystalline LCEs over 4 heat-cool cycles are shown. **(C)** Iso-force tests for semicrystalline LCEs over 4 heat-cool cycles are shown. N = 3 for all tests.

Shape change is also observed when samples are exposed to heat (Figure 9D). Semicrystalline LCEs at room temperature demonstrate an average of 68 ± 7° mm^{-1} twist per length. As the temperature increases, samples start to unwind until they reach a flat state at 100 °C. Upon further increase in temperature, samples start to macroscopically wind again, this time with the twisting

inverted in handedness. The magnitude of shape change at high temperatures is higher than that at room temperature, with the helical ribbon reaching an average of 80 ± 14° mm^{-1} of twist per length with inverted handedness at 200 °C.

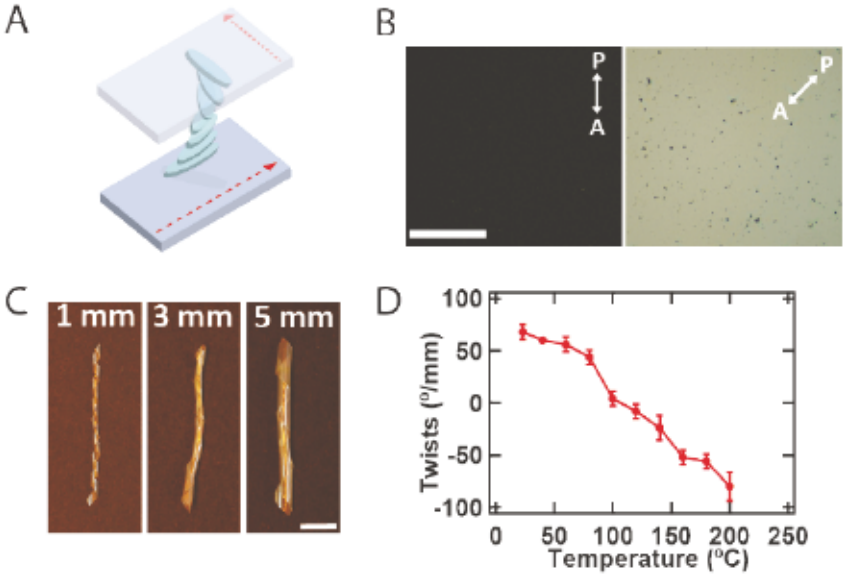

Figure 9. Complex shape-change in semicrystalline LCEs. **(A)** LCE is programmed with an off-axis twist through the thickness of the film. **(B)** Polarized optical microscopy images of samples with twisted nematic alignment under parallel polarizers (Scale bar = 500 μm). **(C)** Aligned semicrystalline LCE adopts a 3D helical configuration at room temperature, with a different number of twists for different widths (Scale bar = 5 mm). **(D)** Twists as a function of temperature for twisted helical samples. For plot D each data point represents the mean (n = 3) and the error bars represent the standard deviation.

Out-of-plane deformation can also be achieved by programming the molecular order in a spatially varied manner around topological defects (Figure 10A).[70,71] Semicrystalline LCEs with director profiles varying radially around a +1 defect, morph into a conical shape at room temperature and an anti-cone when heated up to 180 °C. Patterns with director profiles that vary azimuthally are a saddle-shaped anti-cone at room temperature and a cone when heated up to 180

°C. A 2x3 array of radial defects was patterned into the LCE to demonstrate the load-bearing ability of the films (Figure 10B). Despite being relatively thin (50 μm), the monolithic structure is able to support weight on the apex of the cones, without significant deformation demonstrating a benefit of programmed shape morphing in semicrystalline polymers.

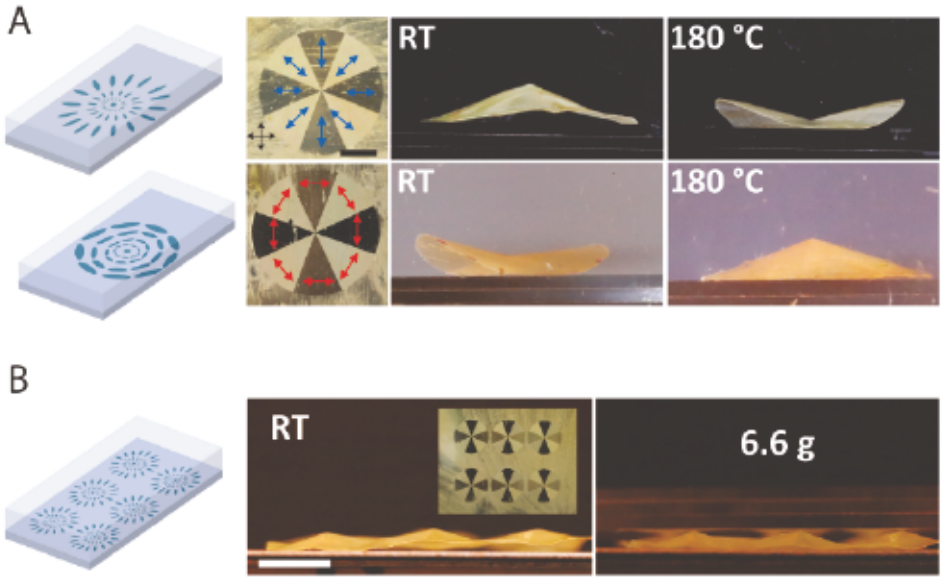

Figure 10. (A) +1 topological defects patterned in semicrystalline LCEs. Radial alignment results in a cone at room temperature and an anti-cone at 180 °C. Azimuthally varied alignment results in an anti-cone at room temperature and a cone at 180 °C (Scale bar = 5 mm). **(B)** An array of cones in a thin film is able to support weight due it its stiff, 3D nature (Scale bar = 5 mm).

4. CONCLUSION

There is a need to develop high-performance engineering materials that are also capable of changing shape. Here, we describe semicrystalline liquid crystal elastomers where the combination of semicrystallinity and liquid crystallinity results in enhanced mechanical properties as well as high deformation strain. The chemistry being employed is amenable to surface

alignment strategies. Complex and spatially varied director profiles within the semicrystalline LCE can result in out-of-plane deformation of thin films such as helical structures, cones, and anti-cones. Semicrystalline LCEs have a modulus of 390 MPa at room temperature, exhibit a contractile blocking force of 2.7 MPa and an actuation strain of 0.56% on heating from 25 ˚C to 50 °C. We envision the use of these tough semicrystalline materials for building LCE-based soft robots and actuators for engineering applications.

For Table of Contents Only

Patterned Shape-change in Semicrystalline Polymers

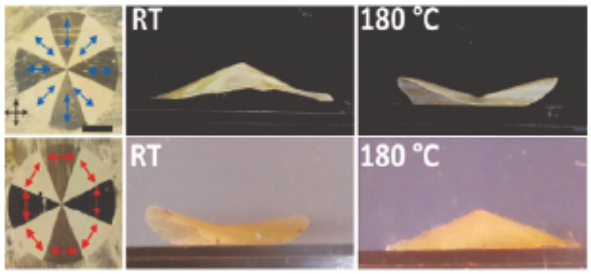

AUTHOR INFORMATION

Corresponding Author

Taylor H. Ware - *Department of Biomedical Engineering, Department of Materials Science and Engineering Texas A&M University, College Station, Texas 77840, United States;*

Email: taylor.ware@tamu.edu

Authors

Mahjabeen Javed - *Department of Biomedical Engineering, Texas A&M University, College Station, Texas 77840, USA;*

Tyler Corazao - *Department of Materials Science and Engineering, Texas A&M University, College Station, Texas 77840, USA;*

Mohand O. Saed - *University of Cambridge, Cambridge, CB2 1TN, UK;*

Cedric P. Ambulo - *Air Force Research Laboratory, Dayton, Ohio, 45433, USA;*

Yuzhan Li - *University of Science and Technology Beijing, Beijing, 100083, China;*

Michael R. Kessler - *North Dakota State University, Fargo, ND, 58108, USA*

Author Contributions

The manuscript was written through the contributions of all authors. All authors have given approval to the final version of the manuscript.

Funding Sources

This material is partially based upon work supported by the National Science Foundation under Grant Nos. 2041671 and 2147830.

Acknowledgments

Use of the Texas A&M University Soft Matter Facility (RRID:SCR_022482) and contribution of Dr. Phuc Truong are acknowledged. Use of the Texas A&M University X-ray Diffraction Laboratory in the Department of Chemistry is acknowledged.

Supporting Information

Additional details of the chemical composition and characterization data of the LCEs (PDF).

References

1. Hervault, A., Dunn, A. E, Lim, M., Boyer, C., Mott, D., Maenosono, S., & Thanh, N. T. K. Doxorubicin Loaded Dual Ph- and Thermo-Responsive Magnetic Nanocarrier for Combined Magnetic Hyperthermia and Targeted Controlled Drug Delivery Applications. *Nanoscale* 8, 12152–12161 (2016).

2. Wei, M., Gao, Y., Li, X. & Serpe, M. J. Stimuli-responsive Polymers and their Applications. *Polym Chem-uk* 8, 127–143 (2016).

3. Yu, Y., Nakano, M. & Ikeda, T. Directed Bending of a Polymer Film by Light. *Nature* 425, 145–145 (2003).

4. Son, S., Shin, E. & Kim, B.-S. Light-Responsive Micelles of Spiropyran Initiated Hyperbranched Polyglycerol for Smart Drug Delivery. *Biomacromolecules* 15, 628–634 (2014).

5. Boothby, J. M., Kim, H. & Ware, T. H. Shape Changes in Chemoresponsive Liquid Crystal Elastomers. *Sensors Actuators B Chem* 240, 511–518 (2017).

6. Hua, F., Cui, T. & Lvov, Y. M. Ultrathin Cantilevers Based on Polymer–Ceramic Nanocomposite Assembled through Layer-by-Layer Adsorption. *Nano Lett* 4, 823–825 (2004).

7. Löwe, C., Zhang, X. & Kovacs, G. Dielectric Elastomers in Actuator Technology. *Adv Eng Mater* 7, 361–367 (2005).

8. Mao, Y., Ding, Z., Yuan, C., Ai, S., Isakov, M., Wu, J., Wang, T., Dunn, M. L., & Qi, H. J. 3D Printed Reversible Shape Changing Components with Stimuli Responsive Materials. *Sci Rep-uk* 6, 24761 (2016).

9. Liu, C., Qin, H. & Mather, P. T. Review of Progress in Shape-Memory Polymers. *J Mater Chem* 17, 1543–1558 (2007).

10. Li, J., Rodgers, W. R. & Xie, T. Semi-crystalline Two-Way Shape Memory Elastomer. *Polymer* 52, 5320–5325 (2011).

11. Xie, P. & Zhang, R. Liquid Crystal Elastomers, Networks and Gels: Advanced Smart Materials. *J Mater Chem* 15, 2529–2550 (2005).

12. Saed, M. O., Volpe, R. H., Traugutt, N. A., Visvanathan, R., Clark, N. A., & Yakacki, C. M. High Strain Actuation Liquid Crystal Elastomers Via Modulation of Mesophase Structure. *Soft Matter* 13, 7537–7547 (2017).

13. Zotzmann, J., Behl, M., Hofmann, D. & Lendlein, A. Reversible Triple-Shape Effect of Polymer Networks Containing Polypentadecalactone- and Poly(ε-caprolactone)-Segments. *Adv Mater* 22, 3424–3429 (2010).

14. Chung, T., Romo-Uribe, A. & Mather, P. T. Two-Way Reversible Shape Memory in a Semicrystalline Network. *Macromolecules* 41, 184–192 (2008).

15. Behl, M. & Lendlein, A. Actively Moving Polymers. *Soft Matter* 3, 58–67 (2006).

16. Westbrook, K. K., Mather, P. T., Parakh, V., Dunn, M. L., Ge, Q., Lee, B. M., & Qi, H. J. Two-Way Reversible Shape Memory Effects in a Free-Standing Polymer Composite. *Smart Mater Struct* 20, 065010 (2011).17. Wermter, H. & Finkelmann, H. Liquid crystalline elastomers as artificial muscles. *E-polymers* 1, 013 (2001).

17. Wermter, H. & Finkelmann, H. Liquid Crystalline Elastomers as Artificial Muscles. *E-polymers* 1, 013 (2001).

18. White, T. J., Serak, S. V., Tabiryan, N. V., Vaia, R. A. & Bunning, T. J. Polarization-Controlled, Photodriven Bending in Monodomain Liquid Crystal Elastomer Cantilevers. *J Mater Chem* 19, 1080–1085 (2008).

19. Yamada, M., Kondo, M., Mamiya, J., Yu, Y., Kinoshita, M., Barrett, C. J., & Ikeda, T. Photomobile Polymer Materials: Towards Light-Driven Plastic Motors. *Angew Chem-ger Edit* 120, 5064–5066 (2008).

20. Javed, M., Tasmim, S., Abdelrahman, M. K., Ambulo, C. P. & Ware, T. H. Degradation-Induced Actuation in Oxidation-Responsive Liquid Crystal Elastomers. *Crystals* 10, 420 (2020).

21. Terentjev, E. M. & Warner, M. Liquid Crystal Elastomers. *Oxford University Press* (2003).

22. Finkelmann, H., Kock, H. & Rehage, G. Investigations on Liquid Crystalline Polysiloxanes 3. Liquid Crystalline Elastomers — A New Type of Liquid Crystalline Material. *Die Makromolekulare Chemie Rapid Commun* 2, 317–322 (1981).

23. Schuhladen, S., Preller, F., Rix, R., Petsch, S., Zentel, R., & Zappe, H. Iris-Like Tunable Aperture Employing Liquid-Crystal Elastomers. *Adv Mater* 26, 7247–7251 (2014).

24. Herbert, K. M., Fowler, H. E., McCracken, J. M., Schlafmann, K. R., Koch, J. A., & White, T. J. Synthesis and Alignment of Liquid Crystalline Elastomers. *Nat Rev Mater* 7, 23–38 (2022).

25. Ambulo, C. P., Burroughs J. J., Boothby, J. M., Kim, H., Shankar, M. R., & Ware, T. H. Four-Dimensional Printing of Liquid Crystal Elastomers. *Acs Appl Mater Inter* 9, 37332–37339 (2017).

26. Kotikian, A., Truby, R. L., Boley, J. W., White, T. J. & Lewis, J. A. 3D Printing of Liquid Crystal Elastomeric Actuators with Spatially Programed Nematic Order. *Adv Mater* 30, 1706164 (2018).

27. Kowalski, B. A., Guin, T. C., Auguste, A. D., Godman, N. P. & White, T. J. Pixelated Polymers: Directed Self Assembly of Liquid Crystalline Polymer Networks. *Acs Macro Lett* 6, 436–441 (2017).

28. Thomsen, D. L., Keller, P., Naciri, J., Pink, R., Jeon, H., Shenoy, D., & Ratna, B. R. Liquid Crystal Elastomers with Mechanical Properties of a Muscle. *Macromolecules* 34, 5868–5875 (2001).

29. Jiang, H., Li, C. & Huang, X. Actuators Based on Liquid Crystalline Elastomer Materials. *Nanoscale* 5, 5225–5240 (2013).

30. Kowalski, B. A., Tondiglia, V. P., Guin, T. & White, T. J. Voxel Resolution in The Directed Self-Assembly of Liquid Crystal Polymer Networks and Elastomers. *Soft Matter* 13, 4335–4340 (2017).

31. White, T. J. & Broer, D. J. Programmable and Adaptive Mechanics with Liquid Crystal Polymer Networks and Elastomers. *Nat Mater* 14, 1087–1098 (2015).

32. Lu, H.-F., Wang, M., Chen, X.-M., Lin, B.-P. & Yang, H. Interpenetrating Liquid-Crystal Polyurethane/Polyacrylate Elastomer with Ultrastrong Mechanical Property. *J Am Chem Soc* 141, 14364–14369 (2019).

33. Ube, T., Minagawa, K. & Ikeda, T. Interpenetrating Polymer Networks of Liquid-Crystalline Azobenzene Polymers and Poly(Dimethylsiloxane) as Photomobile Materials. *Soft Matter* 13, 5820–5823 (2017).

34. Zhao, Y., Yuan, G. & Roche, P. Blends of Side-Chain Liquid Crystalline Polymers: Towards Self-Assembled Interpenetrating Networks. *Polymer* 40, 3025–3031 (1999).

35. Annapooranan, R., Wang, Y. & Cai, S. Highly Durable and Tough Liquid Crystal Elastomers. *Acs Appl Mater Inter* 14, 2006–2014 (2022).

36. Lin, X., Zou, W. & Terentjev, E. M. Double Networks of Liquid-Crystalline Elastomers with Enhanced Mechanical Strength. *Macromolecules* (2021) doi:10.1021/acs.macromol.1c02065.

37. Kim, H., Boothby, J. M., Ramachandran, S., Lee, C. D. & Ware, T. H. Tough, Shape-Changing Materials: Crystallized Liquid Crystal Elastomers. *Macromolecules* 50, 4267–4275 (2017).

38. Volpe, R. H., Mistry, D., Patel, V. V., Patel, R. R. & Yakacki, C. M. Dynamically Crystalizing Liquid-Crystal Elastomers for an Expandable Endplate-Conforming Interbody Fusion Cage. *Adv Healthc Mater* 9, 1901136 (2020).

39. Ohzono, T., Minamikawa, H., Koyama, E. & Norikane, Y. Impact of Crystallites in Nematic Elastomers on Dynamic Mechanical Properties and Adhesion. *Macromolecules* 54, 8987–8995 (2021).

40. Yang, H., Liu, M., Yao, Y., Tao, P., Lin, B., Keller, P., Zhang, X., Sun, Ying., & Guo, L. Polysiloxane-Based Liquid Crystalline Polymers and Elastomers Prepared by Thiol–Ene Chemistry. *Macromolecules* 46, 3406–3416 (2013).

41. Ware, T. H., Perry, Z. P., Middleton, C. M., Iacono, S. T. & White, T. J. Programmable Liquid Crystal Elastomers Prepared by Thiol–Ene Photopolymerization. *Acs Macro Lett* 4, 942–946 (2015).

42. Yang, H., Buguin, A., Taulemesse, J., Kaneko, K., Mery, S., Bergeret, A., & Keller., P. Micron-Sized Main-Chain Liquid Crystalline Elastomer Actuators with Ultralarge Amplitude Contractions. J Am Chem Soc 131, 15000–15004 (2009).

43. Hoyle, C. E. & Bowman, C. N. Thiol–Ene Click Chemistry. *Angewandte Chemie Int Ed* 49, 1540–1573 (2010).

44. Yakacki, C. M., Saed, M., Nair, D. P., Gong, T., Reed, S. M., & Bowman, C. N. Tailorable and Programmable Liquid-Crystalline Elastomers Using a Two-Stage Thiol–Acrylate Reaction. *Rsc Adv* 5, 18997–19001 (2015).

45. Donnio, B., Wermter, H. & Finkelmann, H. A Simple and Versatile Synthetic Route for the Preparation of Main-Chain, Liquid-Crystalline Elastomers. *Macromolecules* 33, 7724–7729 (2000).

46. Broer, D. J., Hikmet, R. A. M. & Challa, G. In-Situ Photopolymerization of Oriented Liquid-Crystalline Acrylates, 4. Influence of A Lateral Methyl Substituent on Monomer and Oriented Polymer Network Properties of a Mesogenic Diacrylate. *Die Makromolekulare Chemie* 190, 3201–3215 (1989).

47. Beers, D. E. & Ramirez, J. E. Vectran High-performance Fibre. *J Text Inst* 81, 561–574 (2008).

48. Xu, D., Wang, W., Zheng, Y., Tian, S., Chen, Y., Lu, Z., Wang, Y., Liu, K., & Wang, D. Graft Copolymer Elastomers with Polar Polyacrylonitrile as Semicrystalline Side Chains: Excellent Toughness and Healability. Macromolecules 53, 8928–8939 (2020).

49. Warner, M. & Wang, X. J. Elasticity and Phase Behavior of Nematic Elastomers. *Macromolecules* 24, 4932–4941 (1991).

50. Greve, A. & Finkelmann, H. Nematic Elastomers: The Dependence of Phase Transformation and Orientation Processes on Crosslinking Topology. *Macromol Chem Physic* 202, 2926–2946 (2001).

51. Cordoyiannis, G., Lebar, A., Rožič, B., Boštjan, Z., Kutnjak, Z., Žumer, S., Brömmel, F., Krause, S., & Finkelmann, H. Controlling the Critical Behavior of Paranematic to Nematic Transition in Main-Chain Liquid Single-Crystal Elastomers. Macromolecules 42, 2069–2073 (2009).

52. Dey, S., Agra-Kooijman, D. M., Ren, W., McMullan, P. J., Griffin, A. C., & Kumar, S. Soft Elasticity in Main Chain Liquid Crystal Elastomers. Crystals 3, 363–390 (2013).

53. Challa, P. K., Chakraborty, S., Breckon, R., Zhang, C., Pardaev, S., Twieg, R. W., Jákli, A., Sprunt, S. N., & Gleeson, J. T. Viscoelastic Properties of a Branched Liquid Crystal in the Nematic Phase. Liq Cryst 41, 747–754 (2014).

54. Ware, T. H. & White, T. J. Programmed Liquid Crystal Elastomers with Tunable Actuation Strain. *Polym Chem-uk* 6, 4835–4844 (2015).

55. Burghardt, W. R. Molecular Orientation and Rheology in Sheared Lyotropic Liquid Crystalline. *Macro Chemistry Physics* (1998).

56. Gantenbein, S., Masania, K., Woigk, W., Sesseg, J. P. W., Tervoort, T. A., & Studart, A. R. Three-Dimensional Printing of Hierarchical Liquid-Crystal-Polymer Structures. Nature 561, 226–230 (2018).

57. Dreher, S., Zachmann, H. G., Moszner N., Mercoli, P., Zanghellini, G. Chain Orientation in Melt-Extruded Samples of Vectra A, Vectra B, And Blends in Relation to the Mechanical Properties. J Appl Polym Sci 67, 531–545 (1998).

58. Abdelrahman, M. K., Kim, H., Maeng, J., Ondrusek, P. & Ware, T. H. Emergent Surface Topography Enabled by Concurrent Crystallization and Polymerization. *Macromolecules* 53, 2388–2395 (2020).

59. Jang, L. K., Abdelrahman, M. K. & Ware, T. H. Photopatterning Crystal Orientation in Shape-Morphing Polymers. *Acs Appl Mater Inter* 14, 22762–22770 (2022).

60. Traugutt, N. A., Volpe, R. H., Bollinger, M. S., Saed, M. O., Torbati, A. H., Dadivanyan, N., & Yakacki, C. M. Liquid-Crystal Order During Synthesis Affects Main-Chain Liquid-Crystal Elastomer Behavior. *Soft Matter* 13, 7013–7025 (2017).

61. Hanzon, D. W., Traugutt, N. A., McBride, M. K., Bowman, C. N., Yakacki, C. M., & Yu, K. Adaptable Liquid Crystal Elastomers with Transesterification-Based Bond Exchange Reactions. *Soft Matter* 14, 951–960 (2018).

62. Ware, T. H., Biggins, J. S., Shick, A. F., Warner, M. & White, T. J. Localized Soft Elasticity in Liquid Crystal Elastomers. *Nat Commun* 7, 10781 (2016).

63. Hiraoka, M., Nakamura, K., Arase, H., Asai, K., Kaneko, Y., John, S. W., Tagashira, K., & Omote, A. Power-Efficient Low-Temperature Woven Coiled Fibre Actuator for Wearable Applications. *Sci Rep-uk* 6, 36358 (2016).

64. Lee, Y., Choi, S., Kang, B.-G. & Ahn, S. Effect of Isomeric Amine Chain Extenders and Crosslink Density on the Properties of Liquid Crystal Elastomers. *Materials* 13, 3094 (2020).

65. Choy, C. L., Chen, F. C. & Young, K. Negative Thermal Expansion in Oriented. *Journal of Polymer Science Polymer Physics Edition* (1981).

66. Aziz, S., Naficy, S., Foroughi, J., Brown, H. R. & Spinks, G. M. Effect of Anisotropic Thermal Expansion on the Torsional Actuation of Twist Oriented Polymer Fibres. *Polymer* 129, 127–134 (2017).

67. Haines, C. S., Lima, M. D., Li, N., Spinks, G. M., Foroughi, Javad., Madden, J. D. W., Kim, S. H., Fang, S., Andrade, M. J. D., Goktepe, F., Goktepe, O., Mirvakili, S. M., Naficy, S., Lepro, X., OH, J., Kozlov, M. E., Kim, S. J., Xu, X., Swedlove, B. J., Wallacw, G. G. & Baughman, R. H. Artificial Muscles from Fishing Line and Sewing Thread. *Science* 343, 868–872 (2014).

68. Verpaalen, R. C. P., Varghese, S., Froyen, A., Cunha, M. P., Pouderoijen, M. J., Severn, J. R., Bhatti, M. R., Peijs, T., Bastiaansen, C. W. M., Debije, M. G., Engels, T. A. P., & Schenning, A. P. H. J. Fast, Light-Responsive, Metal-Like Polymer Actuators Generating High Stresses at Low Strain. *Matter* 2, 1522–1534 (2020).

69. Sawaa, Y., Ye, F., Urayama, K., & Selinger, J. V. Shape Selection of Twist-Nematic-Elastomer Ribbons. PNAS (2011).

70. Modes, C. D., Bhattacharya, K. & Warner, M. Gaussian Curvature from Flat Elastica Sheets. *Proc Royal Soc Math Phys Eng Sci* 467, 1121–1140 (2011).

71. de Haan, L. T., Sánchez-Somolinos, C., Bastiaansen, C. M. W., Schenning, A. P. H. J. & Broer, D. J. Engineering of Complex Order and the Macroscopic Deformation of Liquid Crystal Polymer Networks. *Angewandte Chemie Int Ed* 51, 12469–12472 (2012).